Testing the performance of one and two box models as tools for risk assessment of particle exposure during packing of inorganic fertilizer

Carla Ribalta[1,2], Antti J. Koivisto[3], Ana López-Lilao[4], Sara Estupiñá[4], María C. Minguillón[1], Eliseo Monfort[4], Mar Viana[1].

[1]Institute of Environmental Assessment and Water Research (IDÆA-CSIC), C/ Jordi Girona 18, 08034 Barcelona, Spain.

[2]Barcelona Univeristy, Chemistry Faculty, C/ de Martí i Franquès, 1-11, 08028 Barcelona, Spain

[3]National Research Centre for the Working Environment, Lersø Parkallé 105, Copenhagen DK-2100, Denmark.

[4]Institute of Ceramic Technology (ITC)- AICE - Universitat Jaume I, Campus Universitario Riu Sec, Av. Vicent Sos Baynat s/n, 12006 Castellón, Spain.

Highlights:

- Occupational exposure to particles during industrial packing was assessed.
- No significant increases were found during packing of a granulate fertilizer.
- One and two box models predicted adequately actual worker exposure.
- Including outdoor concentrations in models was seen to improve their performance.
- Models parametrization was seen to be a key issue to adequately predict exposure.

Abstract

Modelling of particle exposure is a useful tool for preliminary exposure assessment in workplaces. However, actual exposure measurements are needed to assess models reliability. Worker exposure was monitored during packing of a complex inorganic granulate fertilizer at industrial scale using small and big bags. Particle concentrations were modelled with one and two box models, where the emission source was estimated with the fertilizer's dustiness index. The exposure levels were used to calculate inhaled dose rates and test accuracy of the exposure modellings. The particle

number concentrations were measured from worker area by using a mobility and optical particle sizer which were used to calculate surface area and mass concentrations. The concentrations in the worker area during pre-activity ranged from 63797 - 81073 cm^{-3}, $4.6x10^6$ to $7.5x10^6$ um^2 cm^{-3}, and 354 to 634 µg m^{-3} (respirable mass fraction) and during packing from 50300 to 85949 cm^{-3}, $4.3x10^6$ to $7.6x10^6$ um^2 cm^{-3}, and 279 to 668 µg m^{-3} (respirable mass fraction). Thus, the packing process did not significantly increase the exposure levels. High particle number concentration was partly due to the use of diesel-powered forklifts. The particle surface area deposition rate in respiratory tract was up to $7.6x10^6$ μm^2 min^{-1} during packing, with 52% - 61% of deposition occurring in the alveolar region. Ratios of the modelled and measured concentrations were 0.98 ± 0.19 and 0.84 ± 0.12 for small and big bags, respectively, when using the one box model, and 0.88 ± 0.25 and 0.82 ± 0.12, respectively, when using the two box model. The modelling precision improved for both models when outdoor particle concentrations were included. This study shows that exposure concentrations during packing of fertilizers can be predicted with a reasonable accuracy by using a concept of dustiness and mass balance models.

Keywords: indoor aerosol modelling, exposure prediction, occupational exposure, industrial packing, risk management.

1. Introduction

Industrial bag filling, packing and pouring processes have been pointed out as activities with high potential to emit airborne particles. Studies in different industrial sectors had reported high levels of worker exposure to particles, e.g; during pouring and packing of paint pigments, packing of TiO_2, carbon black, fullerenes and carbon nanofibres (Ding et al., 2017; Fujitani et al., 2008; Koivisto et al., 2015, 2012a; Koponen et al., 2015; Kuhlbusch et al., 2004, Evans et al., 2010) as well as packing and pouring of cement materials (Notø et al., 2018; Peters et al., 2008). Additionally, differences in particle

54 release have been observed when pouring different materials, different amounts, and
55 using different types of mixing tanks (Koponen et al., 2015). Thus, every case is
56 specific and further research is needed in order to understand emission patterns during
57 packing and pouring.

58 Exposure to particulate matter (PM) is known to cause various adverse health effects,
59 such as pulmonary and cardiovascular diseases and cancer (Landrigan et al., 2017).
60 Current epidemiological and toxicological studies consider $PM_{2.5}$ (with aerodynamic
61 particle diameter $D_p \leq 2.5$ µm) as the most harmful component for human health
62 (Gakidou et al., 2017; Landrigan et al., 2017; World Health Organization, 2016).
63 Inorganic complex fertilizers have been found to be moderately toxic to earthworms
64 (Shruthi et al., 2017). In humans, due to inhalation of fertilizer degradation products,
65 health effects might come up especially after long term exposures (Yara Iberian S.A,
66 2005). Ammonium nitrate, used in complex inorganic fertilizers, when inhaled, was
67 seen to cause possibly meaningful pulmonary function changes (Kleinman et al., 1980)
68 and to be irritating, cause coughing, bronchospasm, laryngospasm and laryngeal
69 edema even at low concentrations (Gorguner and Akgun, 2003). Additionally, the
70 clinical examination of workers of the ammonium nitrate production showed frequent
71 cases of chronic bronchitis and radiculoneuropathy (Tsimakuridze et al., 2005). On the
72 other hand, ammonium nitrate is known to be potentially explosive when confined.
73 Potassium nitrate, also included in some inorganic fertilizers composition, has been
74 seen to be irritating for the respiratory tract (INCHEM, 2001). Therefore, the study of
75 packing of an inorganic fertilizer is of interest as workers can be exposed to relatively
76 high concentrations of airborne fertilizer particles, which might cause respiratory health
77 effects.
78
79 Exposure prediction models have been proposed as valuable risk assessment tools.
80 Since the initial application of exposure prediction models, several research papers

have been published regarding their theoretical aspects (Ganser and Hewett, 2017; Hewett and Ganser, 2017; Hussein and Kulmala, 2008; Nazaroff, 2004; Nazaroff and Cass, 1989). The two box model is a well-accepted exposure assessment tool in the risk assessment field as, even with its simplified assumptions, it is able to adequately simulate actual conditions for various processes including volatile compounds and PM emissions (Arnold et al., 2017; Jayjock et al., 2011). In the chemical industry, models have been tested in a variety of cases (Nicas, 2016; Sahmel et al., 2009 and references therein). However, when testing the models for PM in actual industrial environments, the number of studies decreases (Arnold et al., 2017; Boelter et al., 2009; Johnson et al., 2011; Jones et al., 2011; Koivisto et al., 2015; Lopez et al., 2015). Recently, Arnold et al. (2017) conducted a study where the one and two box models, were evaluated under highly controlled conditions. Predicted exposure results for three industrial solvents when using near and far field models was categorized excellent and good to excellent under the ASTM Standard 5157 criteria (Arnold et al., 2017). However, in order to implement prediction models as trustable tools for worker risk assessment, additional real-world cases need to be evaluated to test model performance and to understand the uncertainties related to critical parameters, such as the source characterization, local controls, and air mixing (Jayjock et al., 2011; Sahmel et al., 2009).

The objectives of the present study were 1) to perform a worker exposure and risk assessment study of packing of an inorganic complex fertilizer in an industrial plant, and 2) to test the one box and two box models performance in real-world settings in order to contribute to the better understanding and validation of exposure prediction models.

2. Methodology

2.1. Work environment and packing process

The measurements were carried out during packing of a fertilizer in two different packing lines between the 23th and 26th of January 2017 at an industrial facility located in Castellón, Spain. The fertilizer (YaraMila COMPLEX, PF595P, YaraIberian S.A.) main components were ammonium nitrate; NH_4NO_3 (15 - 20%), potassium nitrate; KNO_3 (12.5 - 15%) and calcium fluoride; CaF_2 (2 - 3%). The fertilizer was granulated in 2.5 to 5 mm diameter spherical pellets.

The packing hall was only naturally ventilated and the replacement air came from outdoors and from adjacent industrial hall via doors, which were always open (Figure 1). The packing lines were for small bags (25 kg) and big bags (600 kg) where the studied fertilizer was poured into the bags from a silo by using a feed funnel. Figure S1 in the Supporting Information shows photos from the packing lines. The two packing lines were not operated at the same time. Two-day measurements were conducted at both packing lines, small bags day 1 (SB1), small bags day 2 (SB2), big bags day 1 (BB1) and big bags day 2 (BB2). In small bags, packing was carried out through an opening fitting the bag width (33-35 cm) and subsequently mechanically sealed. The fertilizer was poured at a flow of 250 kg min^{-1} and the drop height was 5 cm from the feed funnel to the bag opening. Total material drop height was approximately 0.6 m. The packing process was fully automated and the process area was partially enclosed. In big bags, packing was carried out through a cylindrical opening (20 cm diameter) and at a 175 kg min^{-1} flow; material drop height was 20 cm from the feed funnel to the bag opening. Total material drop height was approximately 1.3 m. In that case, the bag was manually closed by the worker, who was standing in front of the bag at approximately 0.5 m distance.

During small and big bags filling, workers tasks were to control and guarantee the correct functioning of the lines as well as to move the filled bags to the storage area using an electric forklift. Occasionally, diesel-powered forklifts were performing truck loading and unloading operations in the hall.

2.2. Aerosol measurements and sampling

Particle number and mass concentrations were monitored in real time in the worker area (WA), indoors, and outdoors (Figure 1). All online instruments were synchronized prior to the measurements and intercompared overnight between experiments. Particle concentrations during packing were measured for approximately two hours. Additionally, 30 minutes of pre-activity concentrations were measured for each day except for BB2.

In the worker are, the instruments were placed on a portable table at approximately 1 m height (instrument inlets being at 1.5 m above the ground level), at 0.5 m from the emission source and 1 m from the worker (Figure 1 and Figure S1, Supporting Information). The monitoring instruments were:

- An electrical mobility spectrometer (NanoScan, SMPS TSI Model 3910; sample flow rate 0.7 l min^{-1}) to measure particle number concentration and particle size distribution in 13 channels from 10 to 420 nm with a 1 minute time resolution
- A Mini Wide Range Aerosol Spectrometer (Mini-WRAS 1371; sample flow rate 1.2 l min^{-1}) to measure particle mass concentration, particle number concentration and particle size distribution from 10 nm to 35 μm in 41 channels with a 1 minute time resolution
- A miniature diffusion size classifier (DiSCmini Matter Aerosol, Testo; sample flow rate 1 l min^{-1}) to measure particle number concentration, mean particle size and alveolar lung deposition surface area (LDSA) in a range of 10 to 700 nm with a 1 minute time resolution

- A Mini Laser Aerosol Spectrometer (Grimm, Mini-LAS 11R; sample flow rate 1.2 l min^{-1}) to measure particle mass concentration from 0.25 to 32 μm in 31 channels with a 1 minute time resolution.

The indoor and outdoor concentrations were monitored by using a DiSCmini and a Grimm Mini-LAS, with the same settings as described above.

During the packing process, particles emitted were collected onto Au grids (Quantifolil ® with 1 μm diameter holes – 4 μm separation of 200 mesh). The grids were attached to polycarbonate filters that were placed in a sampling cassette (SKC INC., USA, inlet diameter 1/8 in. and filter diameter 25 mm). The cassette was connected to a Leland pump with an operating flow rate of 3 l min^{-1}. The morphology and primary particle size of the particles collected were determined using a transmission electron microscope (TEM, Jeol, JEM 1220, Tokyo, Japan) coupled with an energy-dispersive X-ray (EDX) spectrometer.

The worker area particle number size distributions measured by the NanoScan and MiniWras were combined according to Koivisto et al. (2012a) to obtain a wide range for particle size distribution from 10 nm to 35 μm. NanoScan size channels between 11.5 - 86.6 nm were used while channels ranging from 139 nm to 35 μm were taken from the MiniWras. Between 86.6 nm and 139 nm a combined channel (108.6 nm) was created. Upper channels from NanoScan (> 115.5 nm) were not used as it is known to not have a good resolution for particles >200 nm (Fonseca et al., 2016), while MiniWras was seen to not accurately measure particles under 50 nm; therefore, MiniWras lower channels were not used (see Figure S2, Supporting information) and explanation. Here, due to channels cut, ultrafine particles are defined as D_p < 86.60 nm, fine particles as 86.60 nm < Dp < 943.0 nm and coarse particles as > 943.0 nm.

Increases and reductions in exposure during packing when comparing with pre-activity levels were considered statistically significant when the following approach (Asbach et al., 2012; Kaminski et al., 2015) was fulfilled:

Mean concentration during packing > BG ± 3*(σBG)

where BG is the mean temporal background (pre-activity) concentration and σBG is the standard deviation of the background concentration.

2.3. Dustiness

Material dustiness was assessed by using the continuous drop standard method (EN 15051). The continuous drop device, made of stainless steel, consisted of a cylindrical pipe through which air circulated in an upward direction with a volume flow rate of 53 l min^{-1}. Concentric to the cylindrical pipe there was an inner pipe, slightly shorter than the cylindrical pipe, through which material was dropped at a flow rate of 6 to 10 g min^{-1}, so that the powdered material was released into a counter-current airflow (López-Lilao et al., 2015). Total material drop height during the test is approximately 1.2 m. Two sampling heads for inhalable (approximately PST; designed by Institut für Gefahrstoff-Forschung-IGF) and respirable (approximately PM_4; FSP-2, BGIA) fractions were located slightly above the discharge position of the material. Samples for gravimetric measurements of inhalable and respirable fractions were collected on cellulose thimbles, single thickness, 10x50 mm 25/pk and PVC filters of 37 mm and 5 mc of porosity respectively. The experiment, which lasted for 10 minutes, was repeated two times to ensure results repeatability. Between experiment repetitions, the sampling heads for inhalable and respirable fractions were superficially cleaned while the rest of the device was thoroughly cleaned only at the end of the test.

2.4. Exposure modelling

2.4.1. Dispersion models

Exposure modelling was performed by using a one box model (Hewett and Ganser, 2017) and a two box model (Ganser and Hewett, 2017). Figure 2 shows the models schemes and the mass balance equations. The models assume that 1) particles are fully mixed at all times; 2) mass is created by a source inside the plant (near field in two box model) and by concentrations coming from outdoors; 3) there are no other particle losses than the natural ventilation. The models were used to calculate the respirable fraction. Particle losses by sedimentation may be considered negligible for this size fraction.

2.4.2. Emission source

The emission (S) from the packing process is described based on the dustiness index as:

$$S(t) = DI \cdot H \cdot \frac{dM(t)}{dt} \cdot LC \quad (1)$$

where *DI* is the respirable dustiness index of the fertilizer expressed in mg kg^{-1} or particles kg^{-1}, *H* is the handling energy factor for the process, d*M*/d*t* (kg min^{-1}) is the mass flow of the fertilizer, and *LC* is the protection factor of localized controls. The respirable dustiness index of the fertilizer was obtained using the continuous drop method, as it is the method that adapts better to the process under study (Pujara, 1997; Ribalta et al., 2018 under review).

2.4.3. Modelling parametrization

The input parameters needed to run the model and experimentally unavailable in this case study are the handling energy factor (H), local control factors (LC), and the air flow rate (β) between near field (NF) and far field (FF) (for two box model only).

By definition, *H*, links the energy applied during the process with the energy applied during the dustiness test and can range from 0 to 1 (Koivisto et al., 2015; Lidén, 2006; Schneider and Jensen, 2007). Here, *H* was set to 0.5 for small bags because the drop height during small bags packing was ca. half of the drop height in dustiness test. For big bags, *H* was assumed to be 1 as material drop height was similar to dustiness drop height (see 2.1 and 2.4). With regard to local controls (LC), two main controls were detected. For both small and big bags, the bag itself was estimated in this work to reduce particle release by 40% (applied in the emission rate equation as (LC_{bag} = 0.6). In addition, for small bags one box model, the effect of the enclosure was taken into account and applied in the model reducing emission by 50% ($LC_{enclosed}$ = 0.5) (Fransman et al., 2008). Finally, β was estimated after testing the range values reported by Baldwin and Maynard (1998) and Arnold et al. (2017) taking into account the characteristics from our case scenarios. A sensitivity analysis for different β was carried out and is reported in the section below (Table 1). For small bags it was set at 0.75 m^3 min^{-1} (0.0125 m s^{-1}) as the air flow rate was considered to be low due to the enclosure of the packing line (enclosure opening of 1 m^2). In this case, for the two box model, as the effect of the enclosure was introduced by the NF-FF β, the local control regarding the enclosure ($LC_{enclosed}$) in the emission rate equation was suppressed. For big bags, the air flow rate was considered to be higher as there was no enclosure or division between NF and FF, so β was set to 30 m^3 min^{-1} (0.04 m s^{-1}). The model schemes and parameters are listed in Figure 2. The air exchange rate (AER) between indoor and outdoor air was experimentally calculated considering outdoor wind speed during the measurement period (obtained from the local air quality monitoring network), the size of the outdoors door, and the size of the industrial unit. This resulted in a mean air exchange rate of around 7 h^{-1} for the entire period.

2.5. Calculated active surface area and mass concentrations

The particle active surface area was calculated by applying particle size distribution obtained from NanoScan and MiniWras data combination to the equation (2) described in Heitbrink et al. (2009) as in Koivisto et al. (2012b).

$$S = \frac{3\pi\lambda D_b}{C_c(D_b)\delta} \quad (2)$$

where λ is the mean free path for air, 0.066 μm, and δ is the scattering parameter for air, 0.905. D_b is the mobility diameter and C_c the slip correction factor for the corresponding aerodynamic or mobility particle size.

The particle mass was additionally calculated by using mobility particle diameter and effective density as in Koivisto et al. (2012b)

$$m = \rho_{eff} \frac{\pi}{6} D_b^3 \quad (3)$$

where ρ_{eff} is the effective density. As particles density was unknown, 1 g cm^{-3} was assumed for simplicity.

2.6 Calculated regional inhalation dose rate

The inhalation dose of deposited particles in the respiratory system during inspiration and expiration was quantified. The regional inhalation dose rate was obtained by multiplying particle size concentrations on the worker area (NanoScan and MiniWras data combination) by the ICRP human respiratory tract model deposition probability (ICRP, 2011). The respiratory volume used was 25 l min^{-1}, corresponding to male respiration during light exercise (Koivisto et al., 2012b). The regional dose was calculated for head airways, tracheobronchial and alveolar regions by using simplified deposition fraction equations for the ICRP model as described by Hinds (1999). In the

model particles were assumed to be spherical and to preserve their size during inhalation.

3. Results

3.1. Material morphology and characterization

Samples collected onto Au TEM grids were observed and characterized using TEM-EDX. In the samples collected during SB2 (Figure 3a, 3b, 3c, 3d and 3e) and BB1(Figure 3f, 3g, 3h and 3i) experiments, particles which main elements were O, Na, K, Ca, Cr and Zn were detected proving the presence of fertilizer particles in the worker area (Figure 3a, 3b, 3c, 3d 3f, 3g and 3h). A few differences were observed between both samples. Fertilizer particles size was between 1 μm up to > 35 μm in both samples, although in BB1 there was a bigger proportion of bigger particles (Figure 3f) whereas in SB2 a bigger proportion of smaller ones (Figure 3c). Additionally, agglomerates of nanoparticles, with particle size < 50nm and main components O and C, were found on both samples indicating the presence in the worker area of diesel combustible particles, coming from the diesel forklift (Figure 3d, 3e, 3h and 3i). Those agglomerates were occasionally seen in the BB1 samples (Figure 3h and 3i), whereas in the SB2 they were highly abundant (Figure 3c, 3d and 3e) owing to a higher activity of diesel forklifts inside the plant (96.2%; Table 2).

3.2. Dustiness indices

Material dustiness was assessed using the continuous drop method and results were given in terms of inhalable and respirable mass fractions (mg kg^{-1}) gravimetrically analyzed. Following the EN 15051 dustiness classification for continuous drop, the fertilizer under study was classified as a material with low and very low dustiness indices, with 1026 mg kg^{-1} and 16 mg kg^{-1} for inhalable and respirable fractions, respectively.

306 **3.3. Concentrations**

307 **3.3.1. Worker area concentrations**

308 The measurements started 34 to 46 minutes prior to the packing process. Packing
309 lasted between 1 h 20 minutes and 2 h 43 minutes (Table 2). For BB2 no background
310 concentrations could be recorded. During SB1 (Figure S3), total particle number and
311 inhalable mass concentrations during packing were similar to background
312 concentrations (Table 3 and Figure S3). Concentrations of fine particles (100 nm - 1
313 μm) and thoracic and respirable mass concentrations were lower during packing
314 compared with pre-activity levels (Table 3, Figure S3, Supporting information), which
315 resulted from decreasing background concentrations during the pre-activity period (see
316 Figure S3). Thus, it was concluded that during SB1 experiments no significant impacts
317 on particle exposure were detected. Similarly, during SB2 (Figure 4) experiments no
318 statistically significant differences were observed in terms of mass concentrations
319 between the pre-activity and activity periods (Table 3, Figure 4). These results are in
320 agreement with the low dustiness index of the fertilizer material. Conversely, during
321 SB2 total particle number concentration did increase significantly with regard to pre-
322 activity levels (on average for total particle number, 17340 cm^{-3}) (Table 3, Figure 4).
323 This increase may have been linked to diesel emissions from a diesel forklift which
324 operated inside the plant during this period, as will be discussed below. In addition,
325 very few differences were observed in particle size distributions between the pre-
326 activity and activity particle size distributions for SB1 and SB2 (Figure 5a and 5b). In
327 Koivisto et al. (2012a) measurements during packing of TiO_2 into small and large bags
328 did not have an impact on particle concentrations except when opening the enclosed
329 packing machine. Impacts on worker exposure when packing silicon nanoparticles
330 were also not detected probably because the packing line was hermetically sealed
331 (Wang et al., 2012).

During BB1 (Figure 6), particle number and mass concentrations were again similar to pre-activity concentrations, showing slightly higher (non statistically significant) mean concentrations (Table 3).Total particle number concentrations increased by 4876 cm^{-3} and respirable mass concentration by 314 μg m^{-3} (Table 3, Figure 6). During the BB2 (Figure S4) experiments pre-activity concentrations were not available because the activity was initiated before the monitoring instrumentation was ready, and therefore worker exposure can only be discussed comparing with indoor background concentrations. As in the case of SB1 and SB2 very few differences were observed in particle size distribution between the pre-activity and BB1 packing periods. Only slight increases in particles < 30 nm and > 10 μm were observed (Figures 5c). Contrarily, in Koivisto et al. (2012a), packing of TiO_2 into large bags was seen to increase particles > 500 nm. Even so, the present results were to be expected as when classifying the fertilizer according to its dustiness index, it was sorted as a material with very low and low capacity to generate airborne dust for inhalable and respirable fractions, respectively.

As described above, particle number concentrations increased significantly only during two of the four experiments, i.e., SB2 and BB1. However, those increases were not clearly related to the packing activity as no specific relation was seen with the start and stop of the process (Figures 4 and 6). Increases of ultrafine particles in comparison with the background were always below 40000 cm^{-3}, the suggested reference limit value in this specific case (non-biodegradable granular nanomaterials in the range of 1–100 nm and density < 6 kg l^{-1}) (Van Broekhuizen et al., 2012).

Inhalable and respirable mass concentrations did not exceed in any case the limit values for particles not otherwise specified of 10 and 3 mg m^{-3}, respectively (INSH, 2018). Thus, it may be concluded that packing activity of the specific fertilizer did not have a significant impact on worker exposure with regard to particles in the 11.5 nm – 35 μm size range. It should be pointed out that in this study worker exposure

359 concentrations do not correspond strictly to the worker breathing zone (because
360 instruments were not worn by the workers), which are expected to be higher (Koivisto
361 et al., 2015; Koponen et al., 2015). Additionally, the measurements were carried out for
362 a maximum of 2.5 hours and therefore not representative of the 8 hours necessary to
363 calculate the 8 hr time weighted average over a full shift.

364 Packing processes and similar industrial activities such as material pouring have been
365 previously studied among different types of industries with results indicating that
366 packing, pouring or dumping processes usually lead to slight increases in worker
367 exposure concentrations. Packing of carbon black in bags of 25 kg and 1000 kg was
368 shown to increase airborne particles > 400 nm and mass concentrations (Ding et al.,
369 2017; Kuhlbusch et al., 2004). Fullerenes packing increased particle number > 1000
370 nm (Fujitani et al., 2008). Evans et al. (2010) also found that dumping of carbon
371 nanofibers into a drum resulted in an increase of respirable mass concentrations. In the
372 case of the cement industry, Notø et al. (2018) found that packing was associated with
373 an increase of worker exposure to the thoracic mass fraction of 12% and 33% when
374 working less than and more than half a shift, respectively. On the contrary, pouring of
375 cement at a construction site was seen to have highly variable and low percentages of
376 inhalable mass exposure, probably because of workers performing pouring operations
377 also carried out other activities (Peters et al., 2008). In comparison to these studies, the
378 fertilizer packing case presented in this work seemed to have one of the lowest impacts
379 on worker exposure to particle mass and number concentrations.

380 **3.3.2. Outdoor concentrations**

381 The packing hall was connected by two doors (Figure 1) to outdoors and to another
382 industrial unit. In both sites other processes were occasionally ongoing. Thus, influence
383 of outdoors and other processes taking place in the adjacent industrial unit were to be
384 expected. Outdoor particle number concentrations as well as PM_{10} mass were usually

lower or in a similar range as the worker area and indoor concentrations (thoracic mass fraction) (Table S1 and S2, Supporting information). Regarding mean particle size, it was usually smaller in the outdoor location than in the indoor and worker area by 10 - 20 nm (Table S1, Supporting information) due to the influence of outdoor traffic emissions. Mean particle size remained more or less constant between pre-activity and packing periods in the worker area (38-32, 28-37, 33-37, 41-44 nm), indoor (43-37, 38-43 nm) and outdoor (23-20, 31-31, 29-32 nm) measurement points for all days. In general, outdoor concentrations seemed to follow a different pattern from the rest of the locations even if with some exceptions where similar peaks in outdoor, indoor and worker area were observed (e.g., Figure 4, 11:30; Figure S3, 15:10; Figure S4, 12:15). Numerous studies have reported the infiltration of outdoor particles into diverse indoor environments, especially through windows and doors when they are open (Bennett and Koutrakis, 2006; Hussein et al., 2009; Koponen et al., 2001; Reche et al., 2014; Rivas et al., 2015; Wang et al., 2010). In Wang et al. (2010), outdoor infiltration was detected in a similar packing industrial unit where indoor and outdoor areas were connected by opened doors as in the present study.

3.3.3. Forklifts activity

Electric and diesel forklift activity was recorded and is shown on the top of Figures 4, 6, S3 and S4 and as a percentage of total recorded time in Table 2.

During the SB1 packing period, an increase in particle number concentration (< 50 nm) was detected when the diesel forklift was driving inside the hall (> 15:00 h) (Figure S3a and S3b). During SB2, only a slight increase in number concentration was observed when the diesel forklift was driving and the electric forklift ended its activity (Figure 4a and 4b, 11:10). During BB1, a slightly increase of particle number concentration (mean size 30 nm) was observed coinciding with the start of a diesel forklift at 10:20 (Figure 6a and 6b). During BB2 (Figure S4), two increments of number concentration were

411 detected, but only the first one could be clearly linked to a diesel forklift activity. On
412 some occasions, increases in particle number concentrations in the worker area and
413 indoor seemed to be related to the use of the diesel forklift while in others this
414 relationship was more difficult to establish. For example, the highest statistically
415 significant increase in mean particle number concentration in the worker area was for
416 SB2, also having the highest percentage of diesel forklift activity 96.2% (Table 2).
417 Moreover, when an increase in number concentration linked to the activity of a diesel
418 forklift was seen in the worker area it was also seen in the outdoor and indoor
419 measurement points. This is probably due to the fact that the diesel forklift was used to
420 load and unload trucks, which means that the forklift was moving from outdoor to
421 indoor having to drive by all the measurement points (worker area, indoor and outdoor).
422 Diesel and propane forklifts have been previously identified as a common source of
423 ultrafine particles (20 – 50 nm) in activities such as warehouse bagging and packing
424 (Ding et al., 2017; Huang et al., 2010; Kuhlbusch et al., 2004; Tsai et al., 2011; Viitanen
425 et al., 2017; Wang et al., 2010).

426 Finally, in terms of particle mass concentration, no increases when comparing to pre-
427 activity were detected for any of the four days as discussed before. However, during
428 the SB2 packing period, two peaks at 10:40 and 11:30 (Figure 4b) of particles at
429 around 1 µm which coincided with the start of an electric forklift were identified. Huang
430 et al. (2010) observed during packing of large bags (800 kg) that forklift activity
431 released considerable amounts of dust through particle resuspension. In the present
432 case, this phenomenon was only observed on one occasion, and therefore, no clear
433 relationship can be deduced between electric forklift activity and particle mass
434 concentration increases due to resuspension.

435

436

3.3. Exposure and risk assessment - Regional inhalation dose rates

Inhalation dose rates were estimated for each day using combined data from NanoScan and MiniWras (Table 3 and S3). Particle number dose rates ($\dot{n}$) during packing ranged between 682×10^6 and 1122×10^6 min^{-1}. Increases (between 87×10^6 and 240×10^6 min^{-1}) during the packing process were obtained when comparing with pre-activity periods for all days. Surface dose ($\dot{s}$) analysis was calculated as well as respiratory tract deposition percentages. From the total surface area of the deposited particles during packing ($3.3 – 7.6 \times 10^6$ μm^2 min^{-1}), 52 – 61% was estimated to deposit in the alveolar region, 13 – 14% in the trachea bronchi and 25 – 36% in the head airways (Table 3). The percentage for the alveolar region is lower than that found by Wang et al. (2010), who determined the percentage of deposited surface area in the alveolar region to be 80% during packing in a carbon black manufacturing industry. No increases in the total surface deposited area during packing were observed when compared with the pre-activity periods except for SB2. In addition, an increase on the percentage on the alveolar and trachea bronchi regions during packing was observed for SB1, whereas for the rest, percentages remained approximately the same. This increase in number and surface deposited area is most likely due to the diesel forklift activity or another process taking place near the packing area and not due to the packing process itself, which emits coarser particles as described in previous sections. The day with the highest percentage of diesel forklift activity (SB2) showed the highest increase in total surface deposited area (4.6×10^6 and 6.0×10^6 μm^2 min^{-1} for pre-activity and process respectively). Higher percentages of deposited particles were detected in the alveolar and head airways regions. Particles deposition on the tracheobronchial area is dominated by particles with diameters under 10 nm. Here, instruments used have an under limit at around 20 nm. Thus, when analyzing tracheobronchial estimations the previous fact must be considered.

Particle number deposition percentages on the alveolar region ranged between 66 – 69%, similar range as in Wang et al. (2010), who found it to be 64% during packing in a carbon black manufacturing industry. As pointed out in Wang et al. (2010) the use of both metrics, number concentration and surface area, is advisable as, when used separately, different results may be obtained. In Koivisto et al. (2012b) inhalation dose rates as well as percentages of deposited particles in the respiratory tract were calculated for nanoparticle production process in terms of particle number, mass and active surface area. Increases in number concentration and surface area were detected when comparing pre-activity period with process. For that specific case, number concentration was found to be the metric defining better the particles emitted during the process whereas surface area was found to describe process and background particles (Koivisto et al., 2012b).

3.4. Prediction models

Exposure concentrations were modelled using the one and two box models including and excluding outdoor concentrations. Worker area monitored concentrations were compared to one box modelled results, and to FF modelled concentrations when using the two box model, as worker area monitoring instruments were not placed inside the limits of the defined NF area.

As described in section 2.4.3, a sensitivity analysis was carried out to identify the optimal air flow rate between NF and FF (β) in the two box model for this industrial setting. The range of values tested was obtained from the literature (Baldwin and Maynard, 1998; Arnold et al., 2017), and the results of this analysis are summarized in Tables 1 and 4. For small bags, a range of S = 0.006-0.05 m s^{-1}, where S is wind speed inside the plant, corresponding to β = 0.36-3 m^3 min^{-1} was tested. Modelled concentrations were seen to variate between 26 and 38%. On the other hand, for big bags a range of S = 0.0125-0.04 m s^{-1} corresponding to β = 9.4-30 m^3 min^{-1} was tested,

and modelled concentrations were seen to variate less than 5%. Results evidenced that for small bags, higher β (e.g., 3 m^3 min^{-1}) resulted in modelled/measured ratios up to 1.89, whereas lower β largely underestimated modelled concentrations (ratios = 0.39-0.69 for β = 0.36 m^3 min^{-1}). As a result, a β of 0.75 m^3 $min^{-1}$was selected for the small bag scenarios. In a similar analysis, for the big bag scenarios β was 30 m^3 min^{-1} (Table 1), although as explained β does not seem to be a critical parameter for this scenario.

With the parametrization selected, for the one box setup including outdoor concentrations, modelled concentrations (325, 404, 759 and 546 μg m^{-3} for SB1, SB2, BB1 and BB2, respectively) (Table 4) were able to reproduce actual exposure measurements (279, 318, 668 and 528 μg m^{-3} for SB1, SB2, BB1 and BB2, respectively) (Table 3). Predicted concentrations were only slightly higher than the measured values (Table 3 and 4). The ratio ($m_{modelled}/m_{measured}$) was 1.22 ± 0.07 for the small bags and 1.09 ± 0.08 for big bags (Table 4). For the two box model including outdoors, modelled concentrations (311, 316, 745 and 538 μg m^{-3} for SB1, SB2, BB1 and BB2, respectively) (Table 4) were higher than measured concentrations with a ratio ($m_{modelled}/m_{measured}$) of 1.05 ± 0.08 for small bags and 1.07 ± 0.07 for big bags (Table 4).

Modelled concentrations without adding outdoor concentrations (Table 4) were generally lower than measured concentrations (and only slightly higher in 2 cases; SB1 one and two box model including outdoor). The ratio ($m_{modelled}/m_{measured}$) for the one box model was 0.98 ± 0.19 for the small bags and 0.84 ± 0.12 for the big bags. The ratio ($m_{modelled}/m_{measured}$) for the two box model was of 0.88 ± 0.25 for the small bags and 0.82 ± 0.12 for big bags. Thus, the model underestimated exposure concentrations when outdoor contributions were not included. Commonly, model testing assumes that the initial concentration is zero and that the supplied air is free of

515 contaminants (Zhang et al., 2009). However, as discussed in section 3.3.2, the
516 infiltration of outdoor contaminants is frequent, especially when having open doors as
517 in this case. In the industrial setting under study, modelled concentrations without
518 including outdoor were underestimated in 6 of the 8 cases. This kind of
519 underestimation has been considered detrimental in risk assessment (Arnold et al.,
520 2017). On the other hand, modelled concentrations when including outdoor slightly
521 overestimated measured concentrations and had higher precision. These more
522 conservative results were considered preferable from a risk assessment point of view.

523 Arnold et al. (2017) highlighted the importance of making the right model selection
524 when applying them to real cases. The use of the two box model in a well-mixed
525 environment can lead to an overestimation of the FF and especially of the NF modeled
526 concentrations, whereas using a one box model to estimate concentrations in a NF-FF
527 environment can lead to an underestimation. In the industrial setting under study, the
528 big bags scenario seemed to be clearly a one box case scenario due to the absence of
529 an enclosure. However, both models provided similar predictions, the one box model
530 resulting in only slightly higher concentrations. In general, overestimation by models
531 has been described for both, one and two box models (Johnson et al., 2011; Koponen
532 et al., 2015; Sahmel et al., 2009).

533 **4. Discussion**

534 Evidently, the results obtained regarding modelled concentrations are highly dependent
535 on model parameters such as the handling energy factor, local controls, air exchange
536 rate (AER) and NF-FF air flow (β), which are not yet fully parametrized (Cherrie et al.,
537 2011; Jayjock et al., 2011; Sahmel et al., 2009; Baldwin and Maynard, 1998; Keil and
538 Zhao, 2017) and are often challenging to estimate (Zhang et al., 2009). Sensitivity
539 analyses such as the one presented in Table 1 are also valuable.

In the case of the AER and β, experimental data were not available for this case study and they were thus obtained from the literature and tested by means of a sensitivity analysis. β was seen to be a key parameter when modelling the small bags case scenario while it is not critical for the big bags case scenario. That may be explained by the fact that the small bags case scenario was a real two box case (with an actual enclosure and with a small surface area for the air flow between NF and FF) whereas for the big bags there was no real separation between NF and FF and consequently the theoretical free surface area used in the model was much higher.

Local controls prevent dispersion of the aerosolized particles in the room air or remove the particles from air, e.g. enclosures or local extraction systems (Fransman et al., 2008). When having to consider extractions systems, local control values associated can be relatively easy to determine, but in cases like enclosures or barriers it is more complex especially without having actual exposure concentrations. Local exhaust ventilation efficiency can be calculated by a relatively simple equation (Hewett and Ganser, 2017) although some unknown parameters are required. For cases such as the present study when there is no possibility to experimentally establish a value, Fransman et al. (2008) conducted a review with values proposed for different local controls. Here, enclosure local control and bag protection was included in the equation by using values reviewed in Fransman et al. (2008). The output modelled concentrations were seen to correctly predict measured concentrations when using the reported values.

Finally, the emission source characterization is one of the main sources of uncertainty in the model, as it is strongly case-specific. This is one of the reasons why studies dealing with real-world scenarios are highly necessary in the literature. As in the present study, emission source characterization can be based on the dustiness index which may be obtained by standard methods (Lidén, 2006). However, the handling energy factor must be considered (Koivisto et al., 2015; Lidén, 2006; Schneider and

567 Jensen, 2007). When the dustiness concept cannot be used, equations to estimate
568 emission rates have been described (Hewett and Ganser, 2017; Sachse et al., 2012)
569 and used on real scenarios by using mass equation balance and a convolution theorem
570 (Koivisto et al., 2018a; Koivisto et al., 2018b). However, unlike the other parameters,
571 literature regarding emission rates is still limited.

572 Additionally, an important consideration to be discussed at this point is that the models
573 do not consider particle losses due to sedimentation. Cherrie et al. (2011) found that for
574 particles < 10 μm the impact of deposition might be reasonably ignored, but for
575 particles with a higher aerodynamic diameter the deposition impact may be important.
576 Figure 5 shows that most of the emitted particles during packing were under 10 μm.
577 However, for BB1, a slight increase of particles > 10 μm during packing was observed.

578 Based on the considerations above, it may be concluded that the use of the one box
579 and two box models in the industrial setting tested can satisfactorily predict particle
580 concentrations, especially when input parameters are sufficiently robust. In Sahmel et
581 al. (2009), the steady state model, similar to the one box model used here, was seen to
582 correctly perform concentration modeling when choosing the appropriate factors.
583 However, in industrial settings many considerations must be taken into account and
584 what is clearly observed in a laboratory scale or controlled settings cannot be directly
585 extrapolated to the industrial world. To this end, the parameters used in this work and
586 the coefficients applied, described in section 2.4, may be useful as input for future
587 modelling studies.

588 **5. Conclusions**

589 Packing of a fertilizer into small (respirable fraction range 279-318 μg m^{-3}) and big bags
590 (respirable fraction range 487-668 μg m^{-3}) was not seen to significantly increase worker
591 exposure compared with pre-activity concentrations in terms of inhalable and respirable
592 concentrations. However, increases in particle number concentrations were observed,

quite likely related to the diesel forklift activity. A statistically significant increase in ultrafine particles was observed for SB2 (58646 cm^{-3} during pre-activity; 75912 cm^{-3} during packing). This dataset was used to test the performance of one and two box models as tools for risk assessment under real-world industrial settings.

The one and two box models were tested in a real industrial exposure case scenario, during packing of a fertilizer into small and big bags, with and without enclosure. Both models seemed to be able to predict exposure concentrations. When outdoor concentrations were not included in the models, modelled concentrations slightly underestimated actual concentrations, with ratios modelled/measured ranging between 0.82 ± 0.12 and 0.98 ± 0.19 for the respirable size fraction. The use of outdoor concentrations as an input for the models was seen to improve model performance, resulting in slight overestimations of measured concentrations what was estimated as preferable from a risk assessment point of view. In addition, higher precision between repetitions was achieved when including outdoor contributions (ratio modelled/measured 1.05 ± 0.08 to 1.22 ± 0.07). Thus, it was concluded that including outdoor concentrations in the model resulted in an improved model performance, which may be considered a step forward in the application of risk assessment models.

With regard to the selection of the one or two box models, similar results for the small and big bags case scenarios were obtained. However, slightly better results were obtained when using the two box model for the small bags scenario (one box model 1.22 ± 0.07; two box model 1.05 ± 0.08), whereas both models provided similar results for the big bags (1.09 ± 0.08 and 1.07 ± 0.07 respectively). Thus, it may be concluded that, even in complex real-world settings, the simplest approach of the one box model may provide good results if it is adequately parametrized. Model parametrization is in itself a key issue: the selection of parameters such as the handling energy factor, the local controls and especially the NF-FF air flow in the two box model were seen to be critical for the model's performance. Here, NF-FF air flow, local controls efficiency as

well as handling energy factor were assumed based on literature databases, and relatively accurate predictions were obtained. Therefore, reporting measured or tested values for these parameters is seen as necessary to expand the use and applicability of prediction models for risk assessment.

5. Acknowledgments

This research was founded by the Spanish MINECO (CGL2015-66777-C2-1-R, 2-R), Generalitat de Catalunya AGAUR 2017 SGR41, the Spanish Ministry of the Environment (13CAES006),FEDER (European Regional Development Fund) “Una manera de hacer Europa” and H2020 project caLIBRAte (Work Package 7). M.C. Minguillón acknowledges the Ramón y Cajal Fellowship awarded by the Spanish Ministry of Economy, Industry and Competitiveness. The authors also acknowledge the company Bulk Cargo Logistics S.A for their support. The authors declare no conflict of interest relating to the material presented in this Article.

References

Arnold, S.F., Shao, Y., Ramachandran, G., 2017. Evaluating well-mixed room and near-field–far-field model performance under highly controlled conditions. J. Occup. Environ. Hyg. 14, 427–437.

Asbach, C., Kuhlbusch, T.A.J., Kaminski, H., Stahlmecke, B., Plitzko, S., Götz, U., Voetz, M., Kiesling, H.-J., Dahmann, D., 2012. Standard Operation Procedures For assessing exposure to nanomaterials, following a tiered approach.

Baldwin, P.E.J., Maynard, A.D., 1998. A Sonirvey of Wnnnd Speeds Inn Imioor Workplaces 42, 303–313.

Bennett, D.H., Koutrakis, P., 2006. Determining the infiltration of outdoor particles in the indoor environment using a dynamic model. Aerosol Sci. 37, 766–785.

Boelter, F.W., Simmons, C.E., Berman, L., Scheff, P., 2009. Two-zone model

application to breathing zone and area welding fume concentration data. J. Occup. Environ. Hyg. 6, 289–297.

Cherrie, J.W., MacCalman, L., Fransman, W., Tielemans, E., Tischer, M., Van Tongeren, M., 2011. Revisiting the effect of room size and general ventilation on the relationship between near- and far-field air concentrations. Ann. Occup. Hyg. 55, 1006–1015.

Cousins, C., Boice Jr, J., Cooper, U.J., Lee, U.J., Lochard, K.J., 2011. Annals of the ICRP Published on behalf of the International Commission on Radiological Protection International Commission on Radiological Protection Members of the 2010–2013 Main Commission of ICRP.

Ding, Y., Kuhlbusch, T.A.J., Van Tongeren, M., Jiménez, A.S., Tuinman, I., Chen, R., Alvarez, I.L., Mikolajczyk, U., Nickel, C., Meyer, J., Kaminski, H., Wohlleben, W., Stahlmecke, B., Clavaguera, S., Riediker, M., 2017. Airborne engineered nanomaterials in the workplace—a review of release and worker exposure during nanomaterial production and handling processes. J. Hazard. Mater. 322, 17–28.

European Committee for Standardization (CEN), 2013. Workplace exposure: Measurement of the dustiness of bulk materials; Part1: Requirements and choice of test methods; Part 2: Rotating drum method; Part 3: Continuous drop method (EN 15051). [Stantdard] Brussels, Belgium, 2013.

Evans, D.E., Ku, B.K., Birch, M.E., Dunn, K.H., 2010. Aerosol Monitoring during Carbon Nanofiber Production: Mobile Direct-Reading Sampling. Ann. Occup. Hyg. 54, 514–531.

Fonseca, A.S., Viana, M., Pérez, N., Alastuey, A., Querol, X., Kaminski, H., Todea, A.M., Monz, C., Asbach, C., 2016. Intercomparison of a portable and two stationary mobility particle sizers for nanoscale aerosol measurements. Aerosol

Sci. Tech. 50, 653–668.

Fransman, W., Schinkel, J., Meijster, T., Van Hemmen, J., Tielemans, E., Goede, H., 2008. Development and evaluation of an Exposure Control Efficacy Library (ECEL). Ann. Occup. Hyg. 52, 567–575.

Fujitani, Y., Kobayashi, T., Arashidani, K., Kunugita, N., Suemura, K., 2008. Measurement of the Physical Properties of Aerosols in a Fullerene Factory for Inhalation Exposure Assessment. J. Occup. Environ. Hyg. 5, 380–389.

Global, regional, and national comparative risk assessment of 84 behavioural, environmental and occupational, and metabolic risks or clusters of risks, 1990–2016: a systematic analysis for the Global Burden of Disease Study 2016. Lancet 390, 1345–1422.

Ganser, G.H., Hewett, P., 2017. Models for nearly every occasion: Part II - Two box models. J. Occup. Environ. Hyg. 14, 58–71.

Heitbrink, W.A., Evans, D.E., Ku, B.K., Maynard, A.D., Slavin, T.J., Peters, T.M., 2009. Relationships among particle number, surface area, and respirable mass concentrations in automotive engine manufacturing. J. Occup. Environ. Hyg. 6, 19–31.

Hewett, P., Ganser, G.H., 2017. Models for nearly every occasion: Part I - One box models. J. Occup. Environ. Hyg. 14, 49–57.

Hinds, W.C., 1999. Aerosol technology: Properties, Behavior, and Measurement of Airborne Particles., Wiley-Interscience Publication. Wiley.

Huang, C.H., Tai, C.Y., Huang, C.Y.U., Tsai, C.J., Chen, C.W., Chang, C.P., Shih, T.S., 2010. Measurements of respirable dust and nanoparticle concentrations in a titanium dioxide pigment production factory. J. Environ. Sci. Heal. - Part A Toxic/Hazardous Subst. Environ. Eng. 45, 1227–1233.

695 Hussein, T., Hruška, A., Dohányosová, P., Džumbová, L., Hemerka, J., Kulmala, M.,
696 Smolík, J., 2009. Deposition rates on smooth surfaces and coagulation of aerosol
697 particles inside a test chamber. Atmos. Environ. 43, 905–914.

698 Hussein, T., Kulmala, M., 2008. Indoor Aerosol Modeling: Basic Principles and
699 Practical Applications. Water, Air, Soil Pollut. Focus 8, 23–34.

700 ICSC 0184 - POTASSIUM NITRATE [WWW Document], n.d. URL
701 http://www.inchem.org/documents/icsc/icsc/eics0184.htm (accessed 1.26.18).

702 INSH, 2018. LEP 2018, Instituto Nacional de Seguridad e Higiene en el Trabajo.

703 Jayjock, M.A., Armstrong, T., Taylor, M., 2011. The daubert standard as applied to
704 exposure assessment modeling using the two-zone (NF/FF) model estimation of
705 indoor air breathing zone concentration as an example. J. Occup. Environ. Hyg. 8,
706 D114–D122.

707 Johnson, M., Lam, N., Brant, S., Gray, C., Pennise, D., 2011. Modeling indoor air
708 pollution from cookstove emissions in developing countries using a Monte Carlo
709 single-box model. Atmos. Environ. 45, 3237–3243.

710 Jones, R.M., Simmons, C.E., Boelter, F.W., 2011. Comparing two-zone models of dust
711 exposure. J. Occup. Environ. Hyg. 8, 513–519.

712 Kaminski, H., Beyer, M., Fissan, H., Asbach, C., Kuhlbusch, T.A.J., 2015.
713 Measurements of nanoscale TiO2 and Al2O3 in industrial workplace
714 environments -Methodology and results. Aerosol Air Qual. Res. 15, 129–141.

715 Kleinman, M.T., Linn, W.S., Bailey, R.M., Jones, M.P., Hackney, J.D., 1980. Effect of
716 ammonium nitrate aerosol on human respiratory function and symptoms. Environ.
717 Res. 21, 317–326.

718 Koivisto, A.J., Lyyränen, J., Auvinen, A., Vanhala, E., Hämeri, K., Tuomi, T., Jokiniemi,

719 J., 2012a. Industrial worker exposure to airborne particles during the packing of
720 pigment and nanoscale titanium dioxide. Inhal. Toxicol. 24, 839–849.

721 Koivisto, A.J., Aromaa, M., Mäkelä, J.M., Pasanen, P., Hussein, T., Hämeri, K., 2012b.
722 Concept To Estimate Regional Inhalation Dose of Industrially Synthesized
723 Nanoparticles. ACSNano 6, 1195–1203.

724 Koivisto, A.J., Jensen, A.C.Ø., Kling, K.I., Kling, J., Budtz, H.C., Koponen, I.K.,
725 Tuinman, I., Hussein, T., Jensen, K.A., Nørgaard, A., Levin, M., 2018. Particle
726 emission rates during electrostatic spray deposition of TiO 2 nanoparticle-based
727 photoactive coating. J. Hazard. Mater. 341, 218–227.

728 Koivisto, A.J., Jensen, A.C.Ø., Levin, M., Kling, K.I., Maso, M.D., Nielsen, S.H.,
729 Jensen, K.A., Koponen, I.K., 2015. Testing the near field/far field model
730 performance for prediction of particulate matter emissions in a paint factory.
731 Environ. Sci. Process. Impacts 17, 62–73.

732 Koivisto, A.J., Kling, K.I., Fonseca, A.S., Bluhme, A.B., Moreman, M., Yu, M., Costa,
733 A.L., Giovanni, B., Ortelli, S., Fransman, W., Vogel, U., Jensen, K.A., 2018. Dip
734 coating of air purifier ceramic honeycombs with photocatalytic TiO 2 nanoparticles:
735 A case study for occupational exposure. Sci. Total Environ. 630, 1283–1291.

736 Koponen, I.K., Asmi, A., Keronen, P., Puhto, K., Kulmala, M., 2001. Indoor air
737 measurement campaign in Helsinki, Finland 1999 - The effect of outdoor air
738 pollution on indoor air. Atmos. Environ. 35, 1465–1477.

739 Koponen, I.K., Koivisto, A.J., Jensen, K.A., 2015. Worker exposure and high time-
740 resolution analyses of process-related submicrometre particle concentrations at
741 mixing stations in two paint factories. Ann. Occup. Hyg. 59, 749–763.

742 Kuhlbusch, T.A.J., Neumann, S., Fissan, H., 2004. Number Size Distribution, Mass
743 Concentration, and Particle Composition of PM_1 , $PM_{2.5}$, and PM_{10} in Bag Filling

744 Areas of Carbon Black Production. J. Occup. Environ. Hyg. 1, 660–671.

745 Landrigan, P.J., Fuller, R., Acosta, N.J.R., Adeyi, O., Arnold, R., Basu, N., Baldé, A.B.,
746 Bertollini, R., Bose-O'Reilly, S., Boufford, J.I., Breysse, P.N., Chiles, T., Mahidol,
747 C., Coll-Seck, A.M., Cropper, M.L., Fobil, J., Fuster, V., Greenstone, M., Haines,
748 A., Hanrahan, D., Hunter, D., Khare, M., Krupnick, A., Lanphear, B., Lohani, B.,
749 Martin, K., Mathiasen, K. V, McTeer, M.A., Murray, C.J.L., Ndahimananjara, J.D.,
750 Perera, F., Potočnik, J., Preker, A.S., Ramesh, J., Rockström, J., Salinas, C.,
751 Samson, L.D., Sandilya, K., Sly, P.D., Smith, K.R., Steiner, A., Stewart, R.B., Suk,
752 W.A., van Schayck, O.C.P., Yadama, G.N., Yumkella, K., Zhong, M., 2017. The
753 Lancet Commission on pollution and health. Lancet 391.

754 Lidén, G., 2006. Dustiness testing of materials handled at workplaces. Ann. Occup.
755 Hyg. 50, 437–339.

756 López-Lilao, A., Bruzi, M., Sanfélix, V., Gozalbo, A., Mallol, G., Monfort, E., 2015.
757 Evaluation of the Dustiness of Different Kaolin Samples. J. Occup. Environ. Hyg.
758 12, 547–554.

759 Lopez, R., Lacey, S.E., Jones, R.M., 2015. Application of a Two-Zone Model to
760 Estimate Medical Laser-Generated Particulate Matter Exposures. J. Occup.
761 Environ. Hyg. 12, 309–313.

762 Gorguner, M.A., 2003. Acute inhalation injury. Emerg. Med. Clin. North Am. 21, 533–
763 557.

764 Nazaroff, W.W., 2004. Indoor particle dynamics. Indoor Air 14, 175–183.

765 Nazaroff, W.W., Cass, G.R., 1989. Mathematical modeling of indoor aerosol dynamics.
766 Environ. Sci. Technol. 23, 157–166.

767 Nicas, M., 2016. The near field/far field model with constant application of chemical
768 mass and exponentially decreasing emission of the mass applied. J. Occup.

769 Environ. Hyg. 13, 519–528.

770 Notø, H., Nordby, K.-C., Skare, Ø., Eduard, W., 2018. Job Tasks as Determinants of
771 Thoracic Aerosol Exposure in the Cement Production Industry. Ann. Work Expo.
772 Heal. 62, 88–100.

773 Peters, T.M., Elzey, S., Johnson, R., Park, H., Grassian, V.H., Maher, T.,
774 O'Shaughnessy, P., 2008. Airborne Monitoring to Distinguish Engineered
775 Nanomaterials from Incidental Particles for Environmental Health and Safety. J.
776 Occup. Environ. Hyg. 6, 73–81.

777 Pujara, C.P., 1997. Determination of factors that affect the generation of airborne
778 particles from bulk pharmaceutical powders. PhD diss., Purdue Univeristy, USA.

779 Reche, C., Viana, M., Rivas, I., Bouso, L., Àlvarez-Pedrerol, M., Alastuey, A., Sunyer,
780 J., Querol, X., 2014. Outdoor and indoor UFP in primary schools across
781 Barcelona. Sci. Total Environ. 493, 943–953.

782 Ribalta, C., Viana, M., López-Lilao, A., Estupiñá, S., Minguillón, M.C., Mendoza, J.,
783 Díaz, J., Dahmann, D., Monfort, E., 2018 under review. On the relationships
784 between exposure to particles and dustiness during handling of powders in
785 industrial settings. Ann. Work Expo.

786 Rivas, I., Viana, M., Moreno, T., Bouso, L., Pandolfi, M., Alvarez-Pedrerol, M., Forns,
787 J., Alastuey, A., Sunyer, J., Querol, X., 2015. Outdoor infiltration and indoor
788 contribution of UFP and BC, OC, secondary inorganic ions and metals in PM2.5 in
789 schools. Atmos. Environ. 106, 129–138.

790 Sachse, S., Silva, F., Irfan, A., Zhu, H., Pielichowski, K., Leszczynska, A., Blazquez,
791 M., Kazmina, O., Kuzmenko, O., Njuguna, J., 2012. Physical characteristics of
792 nanoparticles emitted during drilling of silica based polyamide 6 nanocomposites.
793 IOP Conf. Ser. Mater. Sci. Eng. 40, 12012.

794 Sahmel, J., Unice, K., Scott, P., Cowan, D., Paustenbach, D., 2009. The use of
795 multizone models to estimate an airborne chemical contaminant generation and
796 decay profile: Occupational exposures of hairdressers to vinyl chloride in hairspray
797 during the 1960s and 1970s. Risk Anal. 29, 1699–1725.

798 Schneider, T., Jensen, K.A., 2007. Combined Single-Drop and Rotating Drum
799 Dustiness Test of Fine to Nanosize Powders Using a Small Drum. Ann. Occup.
800 Hyg. 52, 23–34.

801 Shruthi N, A.B. and S.M., 2017. Toxic effect of inorganic fertilizers to earthworms
802 (Eudrilus eugeniae). J. Entomol. Zool. Stud. JEZS 5, 1135–1137.

803 Tsai, C.J., Huang, C.Y., Chen, S.C., Ho, C.E., Huang, C.H., Chen, C.W., Chang, C.P.,
804 Tsai, S.J., Ellenbecker, M.J., 2011. Exposure assessment of nano-sized and
805 respirable particles at different workplaces. J. Nanoparticle Res. 13, 4161–4172.

806 Tsimakuridze, M., Saakadze, V., Tsereteli, M., 2005. [The characteristic state of health
807 of ammonia nitrate producing workers]. Georg. Med News 80–83.

808 Van Broekhuizen, P., Van Veelen, W., Streekstra, W.H., Schulte, P., Reijnders, L.,
809 2012. Exposure limits for nanoparticles: Report of an international workshop on
810 nano reference values, in: Annals of Occupational Hygiene. Edinburgh Napier
811 University, pp. 515–524.

812 Viitanen, A.K., Uuksulainen, S., Koivisto, A.J., Hämeri, K., Kauppinen, T., 2017.
813 Workplace measurements of ultrafine particles-A literature review. Ann. Work
814 Expo. Heal.

815 Wang, J., Asbach, C., Fissan, H., Hülser, T., Kaminski, H., Kuhlbusch, T.A.J., Pui,
816 D.Y.H., 2012. Emission measurement and safety assessment for the production
817 process of silicon nanoparticles in a pilot-scale facility. J. Nanoparticle Res. 14,
818 759.

819 Wang, Y.F., Tsai, P.J., Chen, C.W., Chen, D.R., Hsu, D.J., 2010. Using a modified
820 electrical aerosol detector to predict nanoparticle exposures to different regions of
821 the respiratory tract for workers in a carbon black manufacturing industry. Environ.
822 Sci. Technol. 44, 6767–6774.

823 World Health Organization, 2016. Ambient Air Pollution: A global assessment of
824 exposure and burden of disease. World Heal. Organ. 1–131.

825 Zhang, Y., Banerjee, S., Yang, R., Lungu, C., Ramachandran, G., 2009. Bayesian
826 modeling of exposure and airflow using two-zone models. Ann. Occup. Hyg.

827

828 **Figures and Tables**

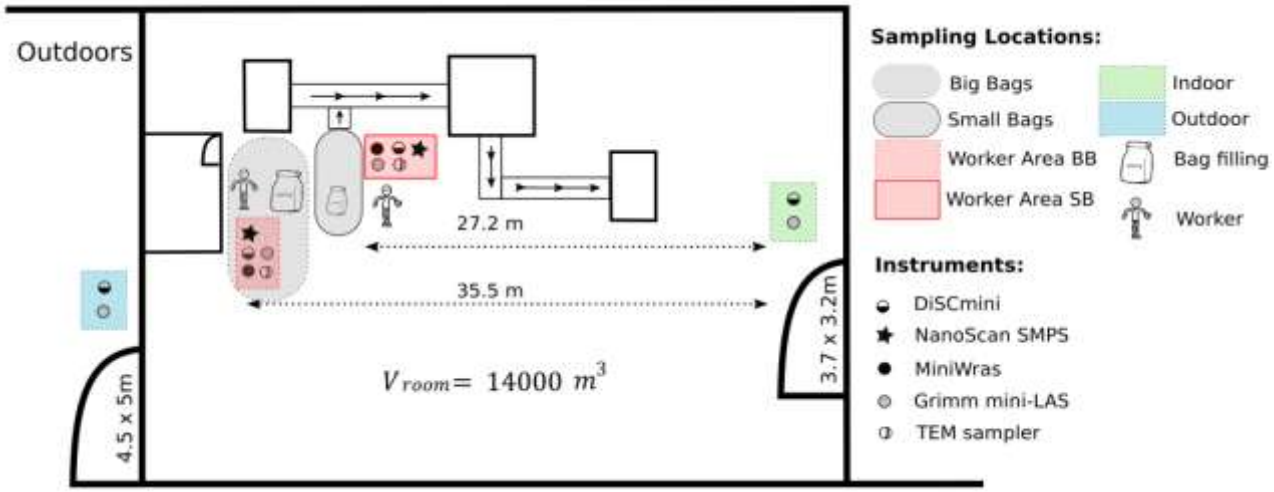

829

830 **Figure 1**. Packing industrial unit layout. Measurement locations as well as devices used during packing
831 operation are pointed out. BB: big bags. SB: small bags.

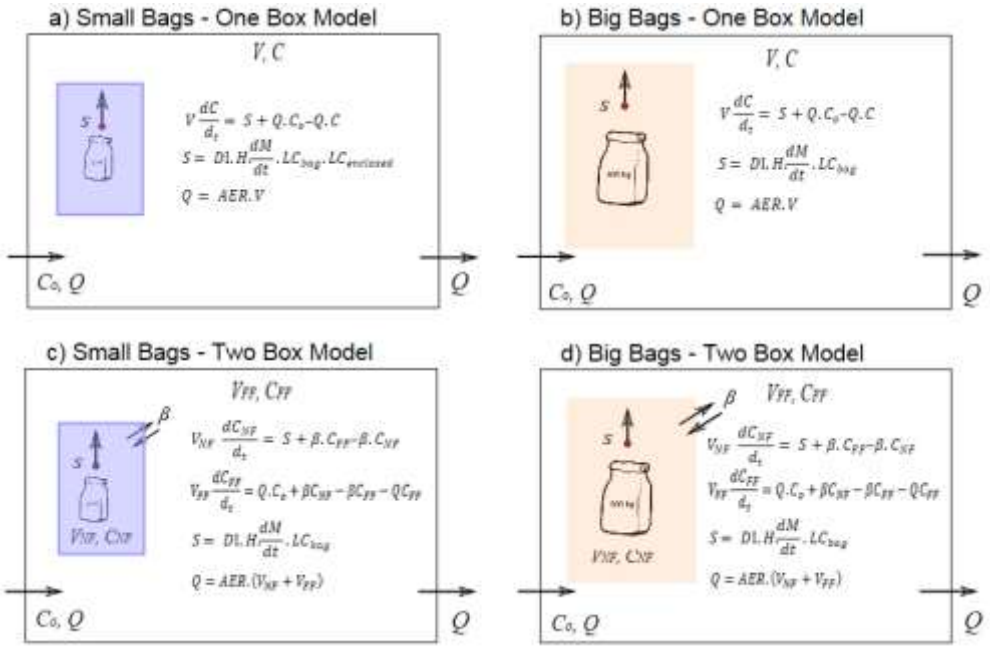

832

SMALL BAGS			
Respirable dustiness index	*DI*	16 mg/kg	Very low dustiness index
Mass flow	*dM/dt*	250 kg/min	Mass flow value
Handling energy	*H*	0.5	Drop height is approximately half of the dustiness test drop height
Local emission controls	LC_{bag}	0.6	0.6 = bag acts as a protection (reduction of the emissions of a 40%)
	$LC_{enclosed}$	0.5	0.5 = process enclosed (reduction of the emissions of a 50%)
Room volume	V_{room}/V_{FF}	14000 m^3	Big industrial unit
Air Exchange rate	*AER*	7 ACH	Medium ventilation rate
Near field volume	V_{NF}	6 m^3	Volume of the enclosed space, it does not include the worker area
Near field air flow	β	0.75 m^3/min	Low air exchange NF-FF (enclosed process)
BIG BAGS			
Respirable dustiness index	*DI*	16 mg/kg	Very low dustiness index
Mass flow	*dM/dt*	175 kg/min	Mass flow value
Handling energy	*H*	1	1 is equivalent to the drop height in the dustiness test
Local emission controls	LC_{bag}	0.6	0.6 = bag acts as a protection (reduction of the emissions of a 40%)
Room volume	V_{room}/V_{FF}	14000 m^3	Big industrial unit
Air Exchange rate	*AER*	7 ACH	Medium ventilation rate
Near field volume	V_{NF}	25m^3	Volume of the bagging line area including worker area
Near field air flow	β	30 m^3/min	High air exchange NF-FF (opened process)

833 **Figure 2**. One box and two box model description and parameters values (table). For small bags, one box
834 model (a) and two box model (c) and for big bags, one box model (b) and two box model (d).

835

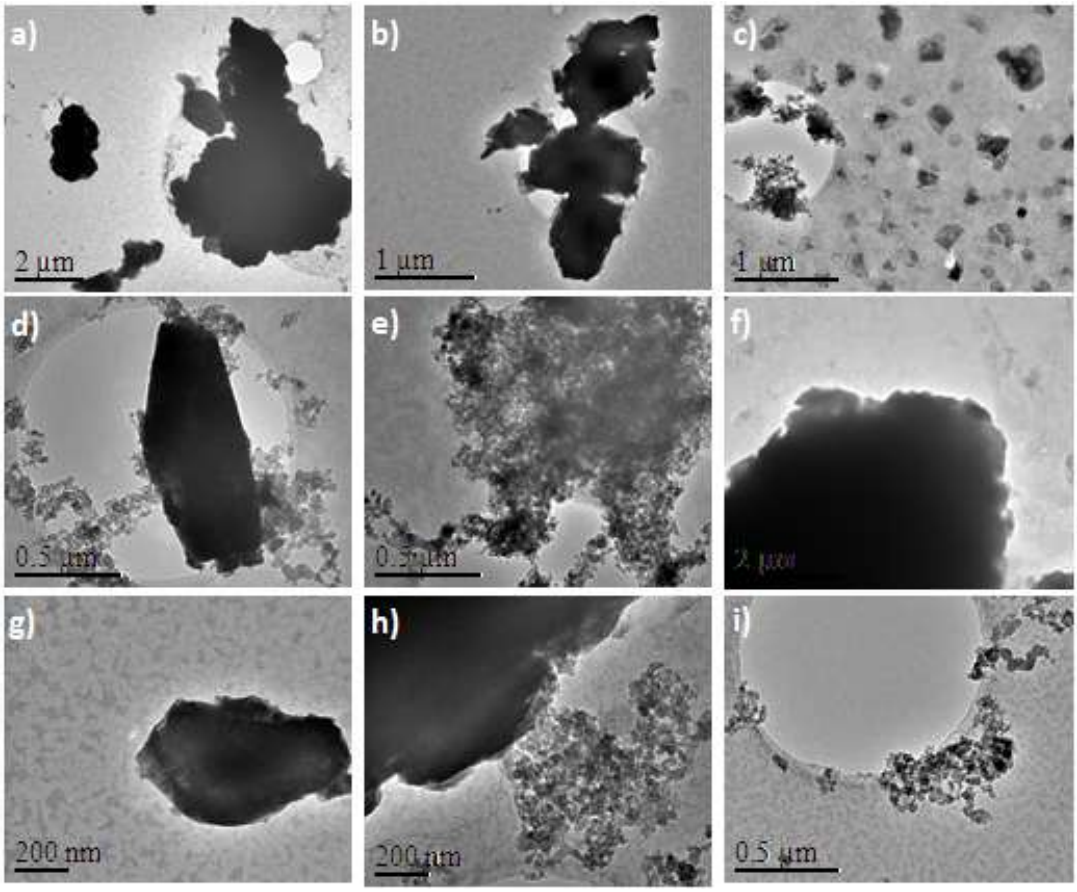

836

837 **Figure 3.** TEM images of the colected particles during the fertilizer bag filling process with small (a, b, c, d
838 and e), and big bags (f, g, h and i).

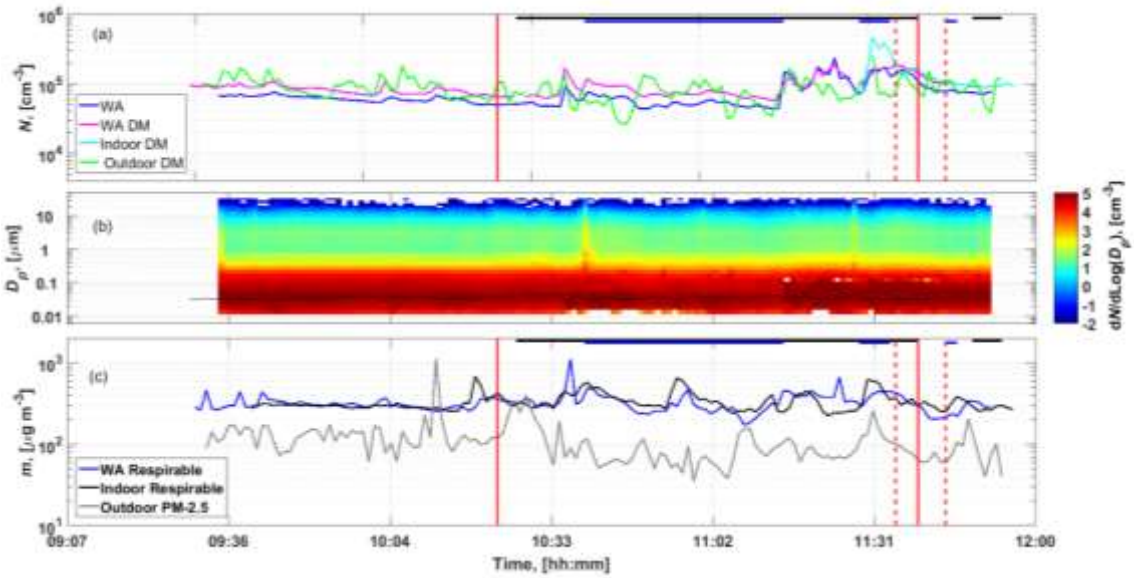

839

840 **Figure 4.** Particle concentration at packing area (WA) during small bags 2 (SB2): (a) particle number
841 concentration time series; (b) particle size distribution time series measured with the MiniWras and the
842 NanoScan, solid black line shows DiSCmini (DM) D_{50}; (c) mass concentration time series. Red vertical

lines indicate start (solid line) and stop (dashed line) of the packing operation and horizontal black and blue lines in the top of the graphs indicate diesel and electric forklifts activity respectively.

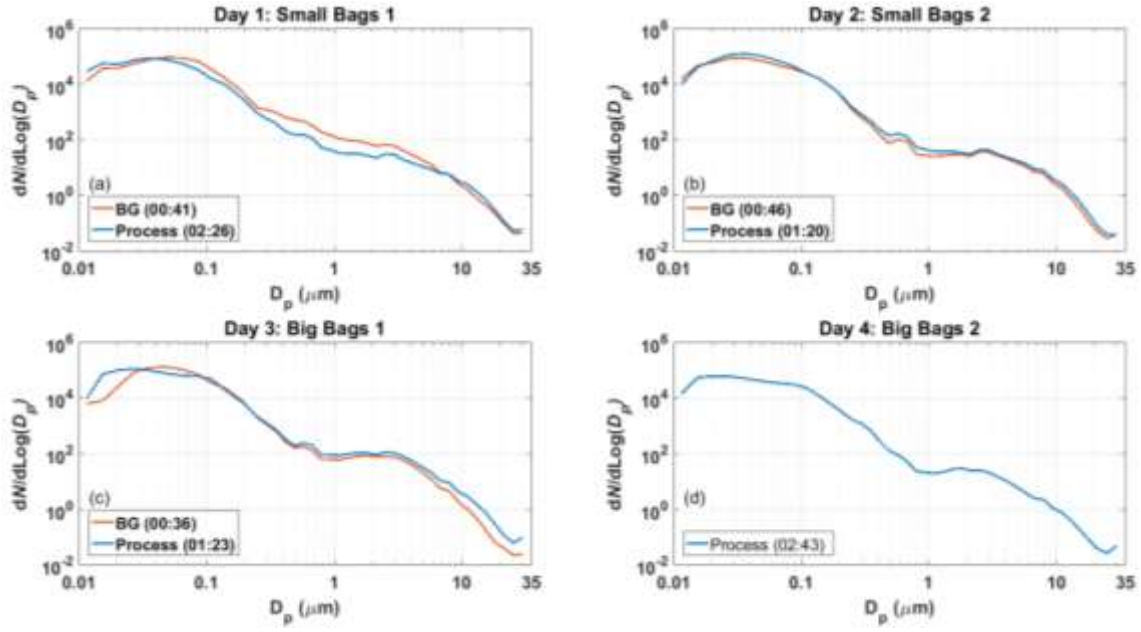

Figure 5. Average particle size distributions measured by NanoScan and MiniWras during pre-activity and packing processes for (a) small bags day 1, SB1; (b) small bags day 2, SB2; (c) big bags day 1, BB1 and (d) big bags day 2, BB2.

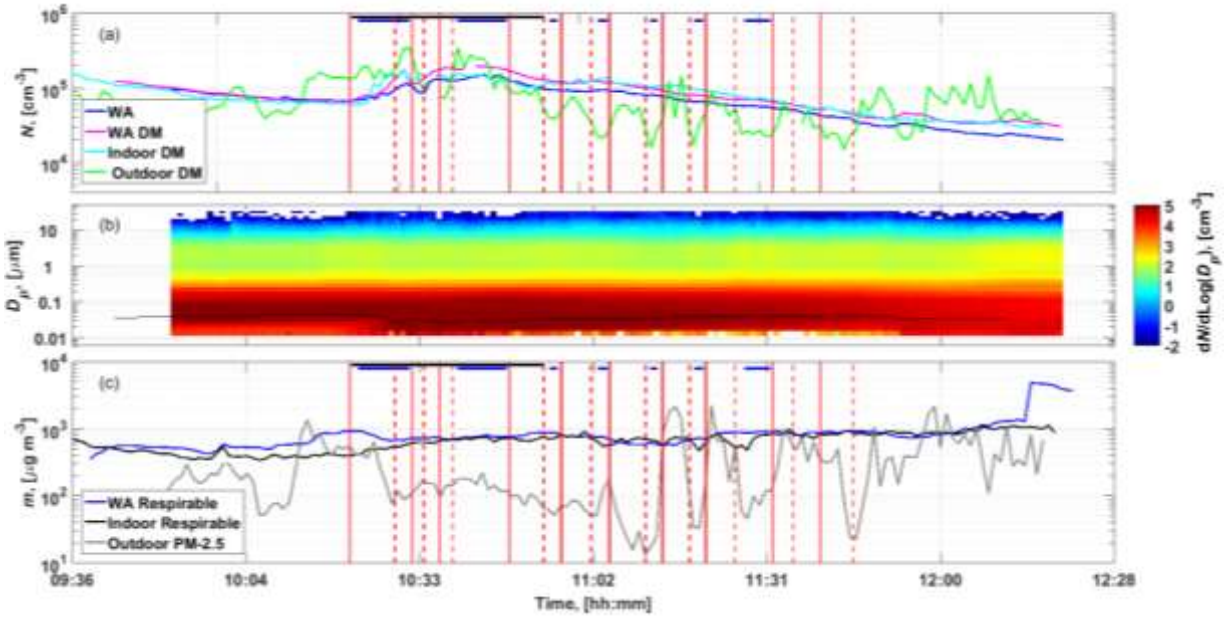

Figure 6. Particle concentration at packing area (WA) during big bags day 1 (BB1): (a) particle number concentration time series; (b) particle size distribution time series measured with the MiniWras and the NanoScan, solid black line shows DiSCmini (DM) D_{50}; (c) mass concentration time series. Red vertical

lines indicate start (solid line) and stop (dashed line) of the packing operation and horizontal black and blue lines in the top of the graphs indicate diesel and electric forklifts activity respectively.

Table 1. Sensitivity analysis for different air flow values for small and big bags with ratios (modelled values/measured values). Variation (%) of the modelled concetration when using the higher and lower air flow value is reported. $\beta = \frac{1}{2}.\ SA\ .S; where\ SA\ is\ the\ surface\ area.$

β (m^3 min^{-1})	S (m s^{-1})	SB1		SB2		β (m^3 min^{-1})	S (m s^{-1})	BB1		BB2	
		With outdoor Ratio	Ratio	With outdoor Ratio	Ratio			With outdoor Ratio	Ratio	With outdoor Ratio	Ratio
0.36	0.006	0.69	0.63	0.68	0.39	-	-	-	-	-	-
0.5	0.004	0.87	0.81	0.81	0.51	-	-	-	-	-	-
0.75	0.0125	1.11	1.06	0.99	0.70	9.4	0.0125	1.08	0.70	0.99	0.88
1	0.017	1.30	1.25	1.15	0.86	12.75	0.017	1.10	0.71	1.00	0.89
1.5	0.025	1.56	1.50	1.40	1.1	15	0.02	1.10	0.71	1.01	0.90
1.8	0.03	1.66	1.60	1.51	1.21	-	-	-	-	-	-
2.4	0.04	1.80	1.75	1.67	1.36	30	0.04	1.12	0.73	1.02	0.91
3	0.05	1.89	1.84	1.79	1.50	-	-	-	-	-	-
Variation (%)		36.4	34.6	38.0	25.8	Variation (%)		3.0	4.5	2.6	2.9

Table 2. Pre-activity, total process time, and total time for each activity (packing, electric forklift and diesel forklift) shown in hh:mm. The percentage of time of each activity (packing, electric forklift and diesel forklift) with respect to the total lenght of the process is included in brackets. Background period (pre-activity) not included. Less than 5 minutes difference between stop and start of the next activity was counted as the same period activity.

Process	Background time	Packing process time	Material pouring time (%)	Electric forklift time (%)	Diesel forklift time (%)
SB1	00:41	02:26	02:03 (84.2%)	00:02 (1.4%)	00:44 (30.2%)
SB2	00:46	01:20	01:16 (95.0%)	00:42 (53.2%)	01:17 (96.2%)
BB1	00:36	01:23	00:46 (55.9%)	00:26 (32.1%)	00:31 (38.4%)
BB2	-	02:43	00:36 (22.1%)	00:40 (24.9%)	02:05 (77.1%)

Table 3. Mean number concentration and mass concentrations during background period (BG) (pre-activity) and packing process in the worker area (WA). N_{TOT} (Dp: 10 nm – 35 µm), N_{UPF} (Dp <; 86.60 nm), N_{FP} (86.60 nm < Dp < 943.0 nm), N_C (Dp> 943.0 nm). Mass concentrations are shown in terms of inhalable, thoracic and respirable fractions measured with the Grimm monitor. Calculated dose rates in particle number, $\dot{n}$, and surface area, $\dot{s}$, and regional deposition in percentages on head airways, trachea bronchi and alveolar. Values in bold indicate statistically significant differences compared with background concentrations.

	Small Bags day 1 (SB1)		Small Bags day 2 (SB2)		Big Bags day 1 (BB1)		Big Bags day 2 (BB2)	
	BG	Packing	BG	Packing	BG	Packing	BG	Packing
N_{TOT} [cm^{-3}]	67254 ± 11076	63108 ± 29592	63797 ± 5435	**81137 ± 42448**	81073 ± 8719	85949 ± 29748	-	50290 ± 40893
N_{UPF} [cm^{-3}]	61083	59900	58646	**75912**	73641	77945	-	46359
N_{FP} [cm^{-3}]	6121	**3188**	5129	5197	7383	7935	-	3922
N_C [cm^{-3}]	50	**20**	22	**28**	50	**68**	-	14
Inhalable [µg m^{-3}]	1987 ± 214	2025 ± 975	1866 ± 1141	1276 ± 550	1650 ± 588	1864 ± 556	-	1047 ± 923
Thoracic [µg m^{-3}]	1487 ± 138	**1053 ± 435**	1147 ± 315	962 ± 345	1183 ± 367	1507 ± 381	-	787 ± 721
Respirable [µg m^{-3}]	634 ± 64	**279 ± 131**	362 ± 74	318 ± 109	354 ± 105	668 ± 153	-	528 ± 898
$\dot{n}_{,\cdot 10^6}$ [min^{-1}]	770	857	834	1035	882	1122	-	682
$\dot{s}_{,\cdot 10^6}$ [µm^2 min^{-1}]	6.4	4.3	4.6	6.0	7.5	7.6	-	3.3
$\dot{s}$,.Head airways [%]	30.7	26.3	27.1	26.2	28.0	36.0	-	24.7
$\dot{s}$,.Trachea bronchi [%]	12.7	14.2	13.9	14.0	13.3	12.5	-	14.2
$\dot{s}$,.Alveolar [%]	56.6	59.5	59.0	59.8	58.7	51.5	-	61.1

875 **Table 4.** One box and two box modeled respirable concentration results including and without including
876 outdoor concentrations. Ratios between modeled and measured concentrations for each specific case are
877 shown in brackets. Last two columns are mean ratio values (and standard deviation) for small and big
878 bags (SB and BB). Last row shows the measured respirable fraction concentrations in the workers area
879 and the spatial background.

[µg/m^3] **(ratio $_{modelled/measured}$)**	SB1	SB2	BB1	BB2	Ratio mean ± (s.d)	
					Small bags	Big bags
One box with outdoor	325 (1.16)	404 (1.27)	759 (1.14)	546 (1.03)	1.22 (0.07)	1.09 (0.08)
Two box with outdoor (FF)	311 (1.11)	316 (0.99)	745 (1.12)	538 (1.02)	1.05 (0.08)	1.07 (0.07)
One box	310 (1.11)	270 (0.85)	501 (0.75)	488 (0.92)	0.98 (0.19)	0.84 (0.12)
Two box (FF)	296 (1.06)	223 (0.70)	487 (0.73)	480 (0.90)	0.88 (0.25)	0.82 (0.12)
Measured respirable fraction in Worker Area	279	318	668	528	-	

880

881